Supporting Information

Non-Equilibrium Dissipation system with Tunable Molecular Fuel Flux

Jiayu Yang,[a] *Tengfang Zhang,*[a] *Linghao Zhang,*[a] *and Xin Su*[*a]

College of Life Science and Technology, Beijing University of Chemical Technology, Beijing 100029, China.

E-mail: xinsu@mail.buct.edu.cn

Contents

Supporting note

Simulation of dynamic microtubule assembly.

To understand how fuel flux affects microtubule assembly, we utilized Python programming to simulate time-dependent microtubule concentration under different fuel flux. The reaction equations and differential equations are summarized as follows:

The reaction equations and differential equations for microtubule assembly in biological systems (with corresponding rate constants and species labeling as depicted in Fig. 1A)

Reaction equations:

$$\mathrm{MF} \xrightarrow{k_G} \mathrm{GTP}$$

$$\mathrm{GTP} + \mathrm{Di} \xrightarrow{k_M} \mathrm{M}$$

$$\mathrm{M} + \mathrm{GDP} \xrightarrow{k_D} \mathrm{Di}$$

Differential equations:

$d[MF]/d[t]=-k_G[MF]$

$d[GTP]/d[t]=k_G[MF]-k_M[GTP][Di]$

$d[Di]/d[t]=-k_M[GTP][Di]+k_D[M][GDP]$

$d[M]/d[t]=k_M[GTP][Di]-k_D[M][GDP]$

$d[GDP]/d[t]=-k_D[M][GDP]$

The assembly rate of microtubules is influenced by factors including the rate of GTP binding to tubulin dimers, the rate of GTP hydrolysis, and the concentration of free tubulin dimers. Under conditions of normal cell growth, to ensure microtubule growth and function,[1,2] the rate of GTP binding to tubulin dimers must exceed the rate of GDP binding, preventing microtubule disassembly from surpassing the assembly rate.[3,4] Following this principle, we set the orders of magnitude for k_G, k_M, and k_D as 10^6 $M^{-1}S^{-1}$, 10^4 $M^{-1}S^{-1}$, and 10^7 $M^{-1}S^{-1}$, respectively. The concentrations of MF, Di, and GDP were 50 nM.

Simulation of DNA-based dissipative systems with fuel flux.

The reaction equations and differential equations for DNA-based dissipative systems with tunable molecular fuel flux (related rate constants and species labels as shown in Fig. 3C)

1. Reaction equations and differential equations for the dissipative system with TMSD-controlled fuel flux.

Reaction equations:

$$I_1 + T_1 \xrightarrow{k_1} F + W2 + R1$$

$$F + R \xrightarrow{k_2} Rep + RF$$

$$RF + \lambda\ Exo \xrightarrow{k_3} RFE$$

$$RFE \xrightarrow{k_4} W1 + R' + \lambda\ Exo$$

$$R' + Rep \xrightarrow{k_5} R$$

Differential equations:

$d[I_1]/d[t]=-k_1\,[I_1][T_1]$

$d[T_1]/d[t]=-k_1\,[I_1][T_1]$

$d[W2]/d[t]=k_1\,[I_1][T_1]$

$d[R1]/d[t]=k_1\,[I_1][T_1]$

$d[F]/d[t]=-k_2\,[F][R]+k_1\,[I_1][T_1]$

$d[R]/d[t]=-k_2\,[F][R]+k_5\,[R'][Rep]$

$d[Rep]/d[t]=k_2\,[F][R]-k_5\,[R'][Rep]$

$d[RF]/d[t]=k_2\,[F][R]-k_3\,[RF][\lambda\ Exo]$

$d[\lambda\ Exo]/d[t]=-k_3\,[RF][\lambda\ Exo]+k_4\,[RFE]$

$d[RFE]/d[t]=k_3\,[RF][\lambda\ Exo]-k_4\,[RFE]$

$d[W1]/d[t]=k_4\,[RFE]$

$d[R']/d[t]=k_4\,[RFE]-k_5\,[R'][Rep]$

2. Reaction equations and differential equations for the dissipative system with Bst reaction-controlled fuel flux.

Reaction equations:

$$I_2 + T_2 \xrightarrow{k_6} I_2T_2$$

$$I_2T_2 + Bst \xrightarrow{k_7} I_2T_2 - Bst$$

$$I_2T_2 - Bst \xrightarrow{k_8} I_2T_2 - Bst + F + W3 + R2$$

$$F + R \xrightarrow{k_2} Rep + RF$$

$$RF + \lambda\ Exo \xrightarrow{k_3} RFE$$

$$RFE \xrightarrow{k_4} W1 + R' + \lambda\ Exo$$

$$R' + Rep \xrightarrow{k_5} R$$

Differential equations:

$d[I_2]/d[t]=-k_6\,[I_2][T_2]$

$d[I_2]/d[t]=-k_6\,[I_2][T_2]$

$d[I_2T_2]/d[t]=k_6\,[I_2][T_2]-k_7\,[I_2T_2][Bst]$

$d[Bst]/d[t]=-k_7\,[I_2T_2][Bst]+k_8\,[I_2T_2\text{-}Bst]$

$d[I_2T_2\text{-}Bst]/d[t]=k_7\,[I_2T_2][Bst]-k_8\,[I_2T_2\text{-}Bst]$

$d[W3]/d[t]=k_8\,[I_2T_2\text{-}Bst]$

$d[R2]/d[t]=k_8\,[I_2T_2\text{-}Bst]$

$d[F]/d[t]=k_8\,[I_2T_2\text{-}Bst]-k_2\,[F][R]$

$d[R]/d[t]=-k_2\,[F][R]+k_5\,[R'][Rep]$

$d[Rep]/d[t]=k_2\,[F][R]-k_5\,[R'][Rep]$

$d[RF]/d[t]=k_2\,[F][R]-k_3\,[RF][\lambda\ Exo]$

$d[\lambda\ Exo]/d[t]=-k_3\,[RF][\lambda\ Exo]+k_4\,[RFE]$

$d[RFE]/d[t]=k_3\,[RF][\lambda\ Exo]-k_4\,[RFE]$

$d[W1]/d[t]=k_4\,[RFE]$

$d[R']/d[t]=k_4\,[RFE]-k_5\,[R'][Rep]$

3. Reaction equations and differential equations for the dissipative system with APE1 reaction-controlled fuel flux.

Reaction equations:

$$T_3 + APE1 \xrightarrow{k_9} T_3 - APE1$$

$$T_3 - APE1 \xrightarrow{k_{10}} F + APE1 + W4 + R3$$

$$F + R \xrightarrow{k_2} Rep + RF$$

$$RF + \lambda\ Exo \xrightarrow{k_3} RFE$$

$$RFE \xrightarrow{k_4} W1 + R' + \lambda\ Exo$$

$$R' + Rep \xrightarrow{k_5} R$$

Differential equations:

$d[T_3]/d[t]=-k_9\,[T_3][APE1]$

$d[APE1]/d[t]=-k_9\,[T_3][APE1]+k_{10}\,[T_3\text{-}APE1]$

$d[T_3\text{-}APE1]/d[t]=-k_{10}\,[T_3\text{-}APE1]+k_9\,[T_3][APE1]$

$d[W4]/d[t]=k_{10}\,[T_3\text{-}APE1]$

$d[R3]/d[t]=k_{10}\,[T_3\text{-}APE1]$

$d[F]/d[t]=k_{10}\,[T_3\text{-}APE1]-k_2\,[F][P]$

$d[R]/d[t]=-k_2\,[F][R]+k_5\,[R'][Rep]$

$d[Rep]/d[t]=k_2\,[F][R]-k_5\,[R'][Rep]$

$d[RF]/d[t]=k_2\,[F][R]-k_3\,[RF][\lambda\ Exo]$

$d[\lambda\ Exo]/d[t]=-k_3\,[RF][\lambda\ Exo]+k_4\,[RFE]$

$d[RFE]/d[t]=k_3\,[RF][\lambda\ Exo]-k_4\,[RFE]$

$d[W1]/d[t]=k_4\,[RFE]$

$d[R']/d[t]=k_4\,[RFE]-k_5\,[R'][Rep]$

The kinetics simulations were established based on the following assumptions:

(1) Enzyme reactions were independent；

(2) The dissociation rate of enzymes was not taken into account；

(3) Enzymatic reactions were irreversible.

Referring to the magnitudes of k values for various reactions as reported in the referenced literature, we defined the respective ranges of variation for k_1 to k_{10} within the system.[5–7] Through individual fittings of the blue curve in Fig. 3D and the gray curves in Fig. 3E and Fig. 3F, we determined all k values, with specific numerical values

detailed in Table S1. In this dynamic model, we employed the standard deviation (σ) between the experimental and fitted curves as a measurement criterion. As the σ value stabilizes, it allows us to identify the unknown *k* values that provide the best fit to the experiment results. During the fitting process, we assume that the enzymes operate under saturated conditions, with substrates tightly interacting with the enzymes.

The difference between the fitted values of critical rate constants (Table S1) and the reported values (Bst exhibits a binding rate constant of 2×10^5 $M^{-1}S^{-1}$, λ Exo has a binding rate constant of 1.16×10^6 $M^{-1}S^{-1}$, and the hybridization rate constant for single strands is 6.48×10^5 $M^{-1}S^{-1}$) are within one order of magnitude.

To align with the unit of species concentration in the simulation, we converted all DNA and enzyme concentrations. Enzyme activity concentrations (U/mL) were transformed into apparent concentrations (nM), for instance, Bst at 160 U/mL corresponds to 0.16 nM. Furthermore, the fluorescence signal is positively correlated with the concentration of free fluorescent strands, and the DNA components can be converted using the following formula: $(F_t-F_{min})/(F_{max}-F_{min})\times[Rep]$, where F_t represents real-time fluorescence intensity, F_{max} and F_{min} respectively denote the fluorescence intensity of free fluorescent strands and hybridized fluorescent strands. [Rep] represents the concentration of Rep strand.

Supporting Tables

Table S1 Rate constants used in the simulation of the non-equilibrium dissipative system with tunable molecular fuel flux

Dissipative system with TMSD-controlled fuel flux	$k_{1\text{-}9}$=8.33x10^5 M^{-1}S^{-1} $k_{1\text{-}10}$=1.167x10^6 M^{-1}S^{-1} $k_{1\text{-}11}$=1.5x10^6 M^{-1}S^{-1} $k_{1\text{-}12}$=1.833x10^6 M^{-1}S^{-1} k_2=3.75x10^4 M^{-1}S^{-1} k_3=9.97x10^7 M^{-1}S^{-1} k_4=0.75 S^{-1} k_5=1.0x10^4 M^{-1}S^{-1}
Dissipative system with Bst reaction-controlled fuel flux	k_6=2.3x10^4 M^{-1}S^{-1} k_7=1.625x10^7 M^{-1}S^{-1} k_8=0.167 S^{-1}
Dissipative system with APE1 reaction-controlled fuel flux	k_9=2.327x10^7 M^{-1}S^{-1} k_{10}=0.0159 S^{-1}

Note: In $k_{1\text{-}x}$, the variable "x" represents the toehold length.

Table S2 The sequences of oligonucleotides

Name	Sequence (5' -3')
	TMSD
1	ACACCTTTAACCCGTACCATTTTTT-FAM
2	GTACCCCTTGCTCCTACTAAACTAA
3	BHQ1- AAAAAATGGTACGGGTTAAAGGTGTTTAGTTTAGTAGGAGCAA GGGGTACCTTCAGGGCCAT

Note: 1, 2, and 3 forms N. M are $I_{1\text{-}9}$, $I_{1\text{-}10}$, $I_{1\text{-}11}$, $I_{1\text{-}12}$.

Name	Sequence (5' -3')
	Bst reaction
4	GGTGTAGAGAAATATGGCCCTGAAG
5	GTACCCCTTGCTCCTACTAAACTAATTTTT
6	BHQ1- AAAAAATGGTACGGGTTAAAGGTGTTTAGTTTAGTAGGAGCAA GGGGTACCTTCAGGGCCATATTTCTCTACACC

Note: 1, 5, and 6 forms Q. P is 4.

Name	Sequence (5' -3')
	APE1 reaction
7	ACACCTTTAACCCGTACCATT-(FAM)TTTT
8	BHQ1- AAAAAATGGTACXGGTTAAAGGTGTTTAGTTTAGTAGGAGCAA GGGGTAC

Note: 2, 7, and 8 forms S. X is the apurinic/apyrimidinic (AP) site for APE1 cleavage.

Name	Sequence (5' -3')
Dissipative system with TMSD-controlled fuel flux	
$I_{1\text{-}9}$	GCCCTGAAGGTACCCCTTGCTCCTACTAAACTAAACACCTTTAACC
$I_{1\text{-}10}$	GGCCCTGAAGGTACCCCTTGCTCCTACTAAACTAAACACCTTTAACC
$I_{1\text{-}11}$	TGGCCCTGAAGGTACCCCTTGCTCCTACTAAACTAAACACCTTTAACC
$I_{1\text{-}12}$	ATGGCCCTGAAGGTACCCCTTGCTCCTACTAAACTAAACACCTTTTAACC
$T_{1\text{-}9}$	A*A*A*A*AATGGTACGGGTTAAAGGTGTTTAGTTTAGTAGGAGCAAGGGGTACCTTCAGGGC
$T_{1\text{-}10}$	A*A*A*A*AATGGTACGGGTTAAAGGTGTTTAGTTTAGTAGGAGCAAGGGGTACCTTCAGGGCC
$T_{1\text{-}11}$	A*A*A*A*AATGGTACGGGTTAAAGGTGTTTAGTTTAGTAGGAGCAAGGGGTACCTTCAGGGCCA
$T_{1\text{-}12}$	A*A*A*A*AATGGTACGGGTTAAAGGTGTTTAGTTTAGTAGGAGCAAGGGGTACCTTCAGGGCCAT
T_1-1	GTACCCCTTGCTCCTACTAAACTAATTTTT
F-1	P- ACACCTTTAACCCGTACCATTTTTT

Note: F-1, $T_{1\text{-}9}$, and T_1-1 forms T_1. In $I_{1\text{-}x}$ and $T_{1\text{-}x}$, the variable "x" represents the toehold length. All sequences listed in the above table are depicted in Fig. 3C.

Name	Dissipative system with Bst reaction-controlled fuel flux
I_2	GGTGTAGAGAAATATGGCCCTGAAG
T_2-1	AAAAAATGGTACGGGTTAAAGGTGTTTAGTTTAGTAGGAGC
	AAGGGGTACCTTCAGGGCCATATTTCTCTACACC

Note: F-1, T_2-1, and T_1-1 forms T_2. All sequences listed in the above table are depicted in Fig. 3C.

Name	Dissipative system with APE1 reaction-controlled fuel flux
T_3-2	GTACCCCTTGCTCCTACTAAACT*A*A
T_3-1	A*A*A*A*AATGGTACXGGTTAAAGGTGTTTAGTTTAGTAGG
	AGCAAGGGGTAC

Note: T_3-2, T_3-1, and F-1 forms T_3. All sequences listed in the above table are depicted in Fig. 3C. X is the AP site.

Name	Strands for dissipative system
R-1	CGTACCATTTTTTTACCTCTTTTTT-FAM/
	CGTACCATTTTTTTACCTCT(FAM)TTTTT
R-2	BHQ1-GCTAGACGCAGATGTACTGTCTGTA
R-3	TACAGACAGTACATCTGCGTCTAGCAGAGGTAAAAAAATGG
	TACGGGTTAAAGGTGT

Note: R-1, R-2, and R-3 forms R. All sequences listed in the above table are depicted in Fig. 3A.

Name	Strands for Assembly and disassembly of AuNPs
$I_{1\text{-}7}$-1	CCTGAAGGTACCCCTTGCTCCTACTAAACTAAACACCT
	TTAACCCGTTTGTGATGGA
$I_{1\text{-}12}$-1	ATGGCCCTGAAGGTACCCCTTGCTCCTACTAAACTAAA
	CACCTTTAACCCGTTTGTGATGGA
T_1-3	GTACCCCTTGCTCCTACTAAACTAA
F-2	P-ACACCTTTAACCGGTTTGTGATGGA
$T_{1\text{-}7}$-1	T*C*C*A*TCACAAACGGGTTAAAGGTGTTTAGTTTAGT
	AGGAGCAAGGGGTACCTT*C*A*G*G
$T_{1\text{-}12}$-1	T*C*C*A*TCACAAACGGGTTAAAGGTGTTTAGTTTAGT
	AGGAGCAAGGGGTACCTTCAGGG*C*C*A*T
R-4	GGTTTGTGATGGACGTTCTTCTGTC
R-5	GCTAGACGCAGATGTACTGTCTGTA
R-6	T*A*C*A*GACAGTACATCTGCGTCTAGCGACAGAAGA
	ACGTCCATCACAAACCGGTTAAAG*G *T*G*T
Au-1	SH-AAAAAAAAAAAAAAAACAGAAGAAC
Au-2	CCATCACAAAAAAAAAAAAAAAAA-SH

Note: **F-2**, **$T_{1\text{-}7}$-1**, and **T_1-3** forms **T_1**. **R-4**, **R-5**, and **R-6** forms **R**. All sequences listed in the above table are depicted in Fig. 4. "*" represents phosphonothioate, and X represents the AP site.

Supporting Fig.s

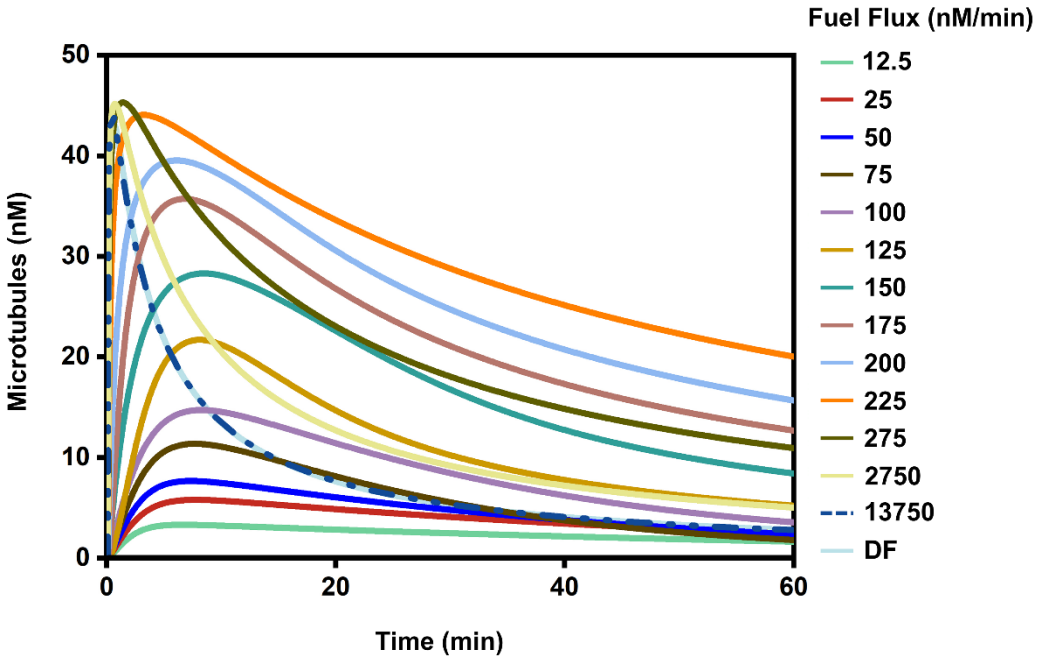

Fig. S1. Simulated oscillatory microtubule concentration mediated by GTP metabolism. The initial concentrations of macromolecule fuel (MF), free tubulin dimer (Di), and GDP were 50 nM.

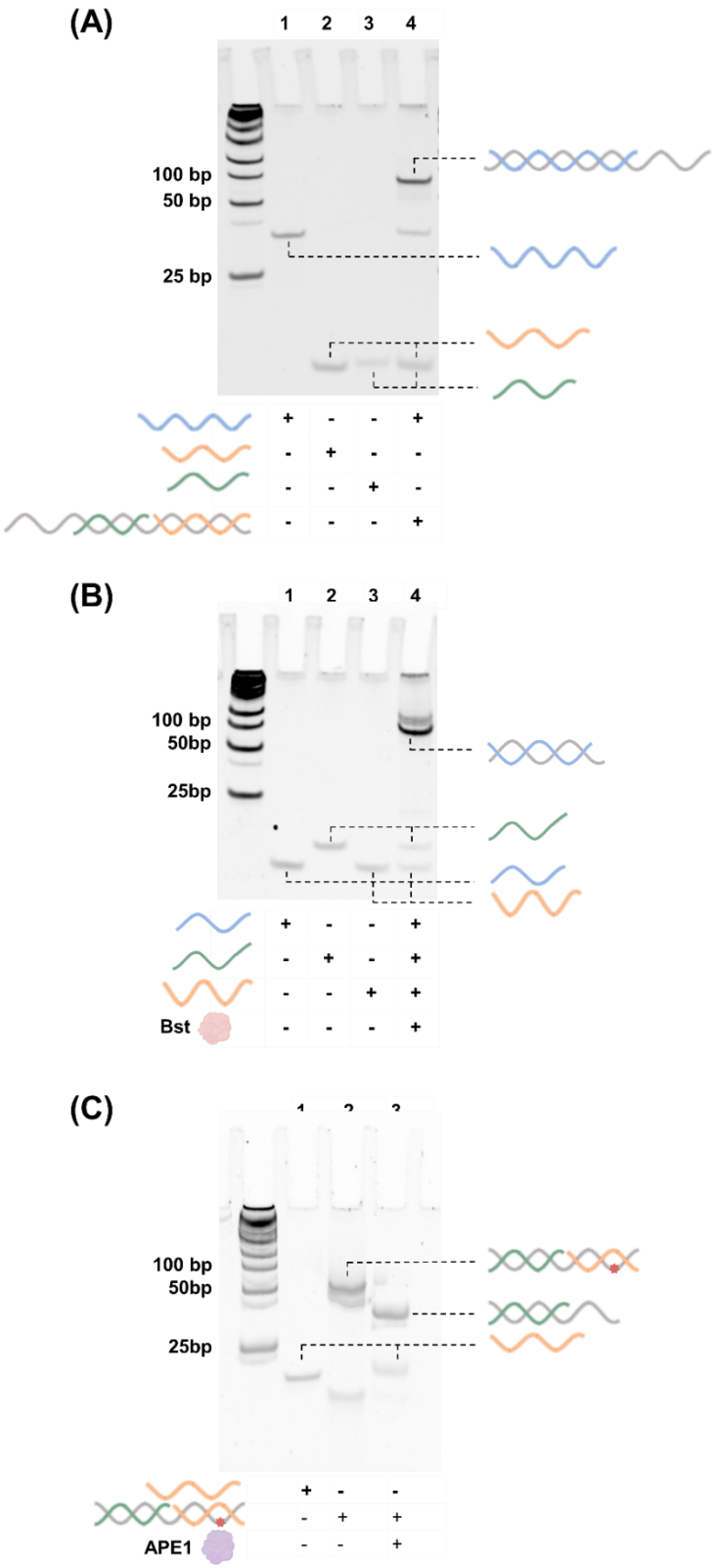

Fig. S2. Characterization of the fuel strand generator by 20% native polyacrylamide gel electrophoresis. (A) TMSD reaction. Lane 4 indicated the release of the fuel strand

(yellow). (B) Bst polymerase reaction. Lane 4 indicated the release of the fuel strand (yellow). (C) APE1 reaction. Lane 3 indicated the release of the fuel strand (yellow).

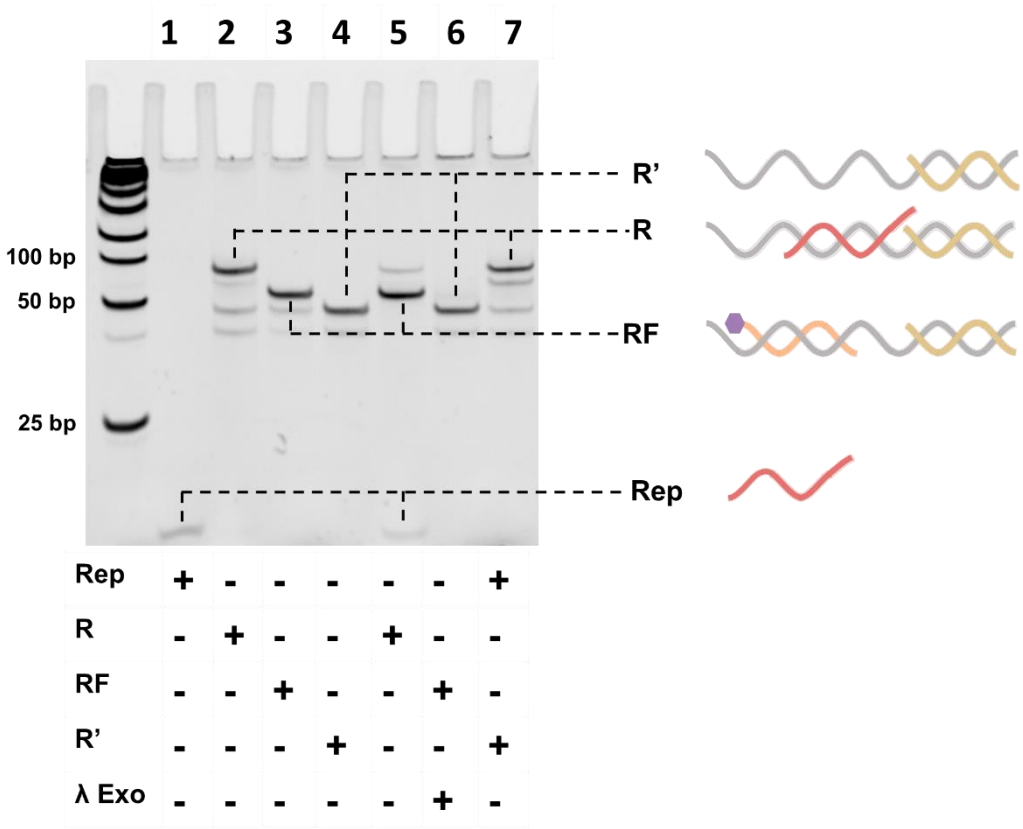

Fig. S3. Characterization of the DNA-based dissipative system by gel electrophoresis. Lane 5 confirmed the release of the Rep strand via the strand displacement reaction between the F and R strands. Lane 6 verified the generation of the R' strand from RF by λ Exo. Lane 7 indicated the re-binding of the R' strand with the Rep strand.

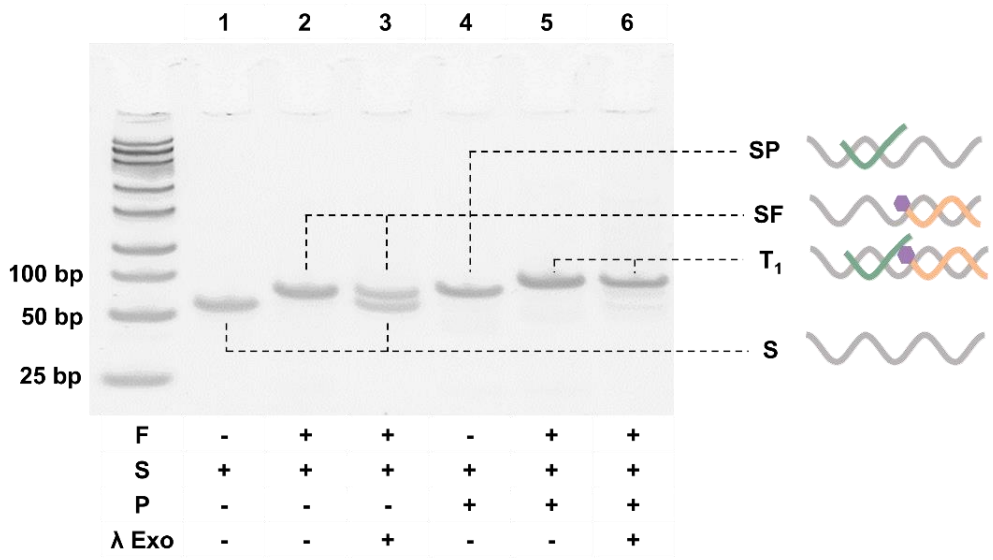

Fig. S4. Characterization of the effect of blocker strand. Lane 3 revealed the release of the S strand through the reaction between the λ Exo and SF strands. Lane 6 indicates that the S strand had not been released, and the P strand functions as a blocking agent. The DNA concentration was 200 nM, the λ Exo concentration was 250 U/mL, and the temperature was 25 ° C.

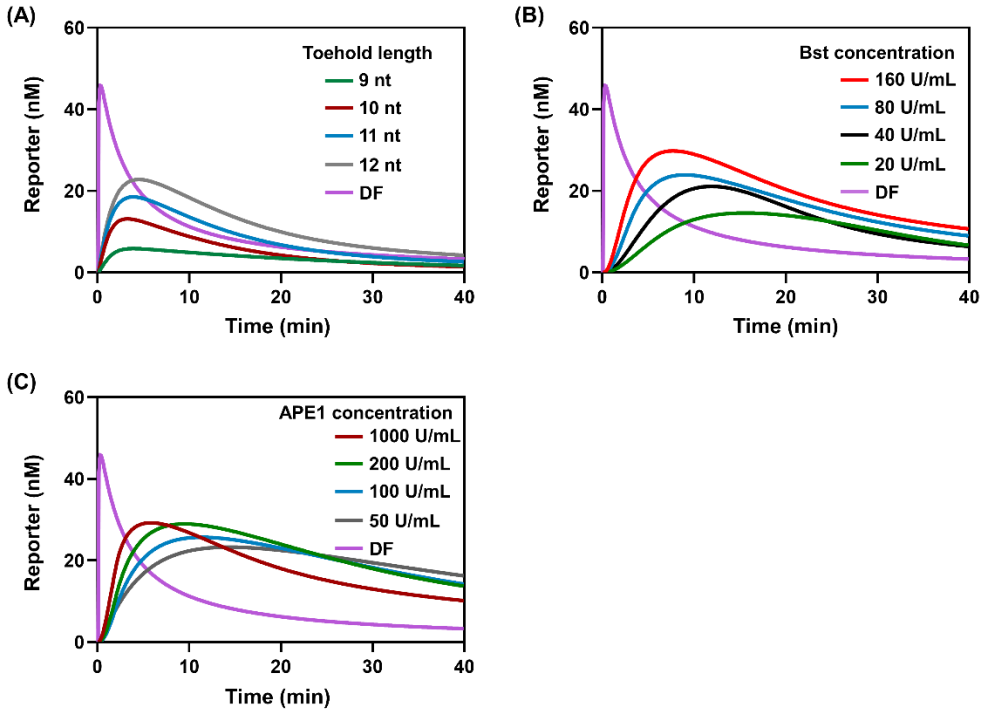

Fig. S5. The simulated time-dependent concentration of the reporter strand in the dissipative systems. (A) Simulation of dissipative system with TMSD-controlled fuel

flux. (B) Simulation of dissipative system with Bst reaction-controlled fuel flux. (C) Simulation of dissipative system with APE1 reaction-controlled fuel flux. The concentration of DNA strands in all reaction systems was 50 nM. All the rate constants *k* in the simulation are shown in Table S1.

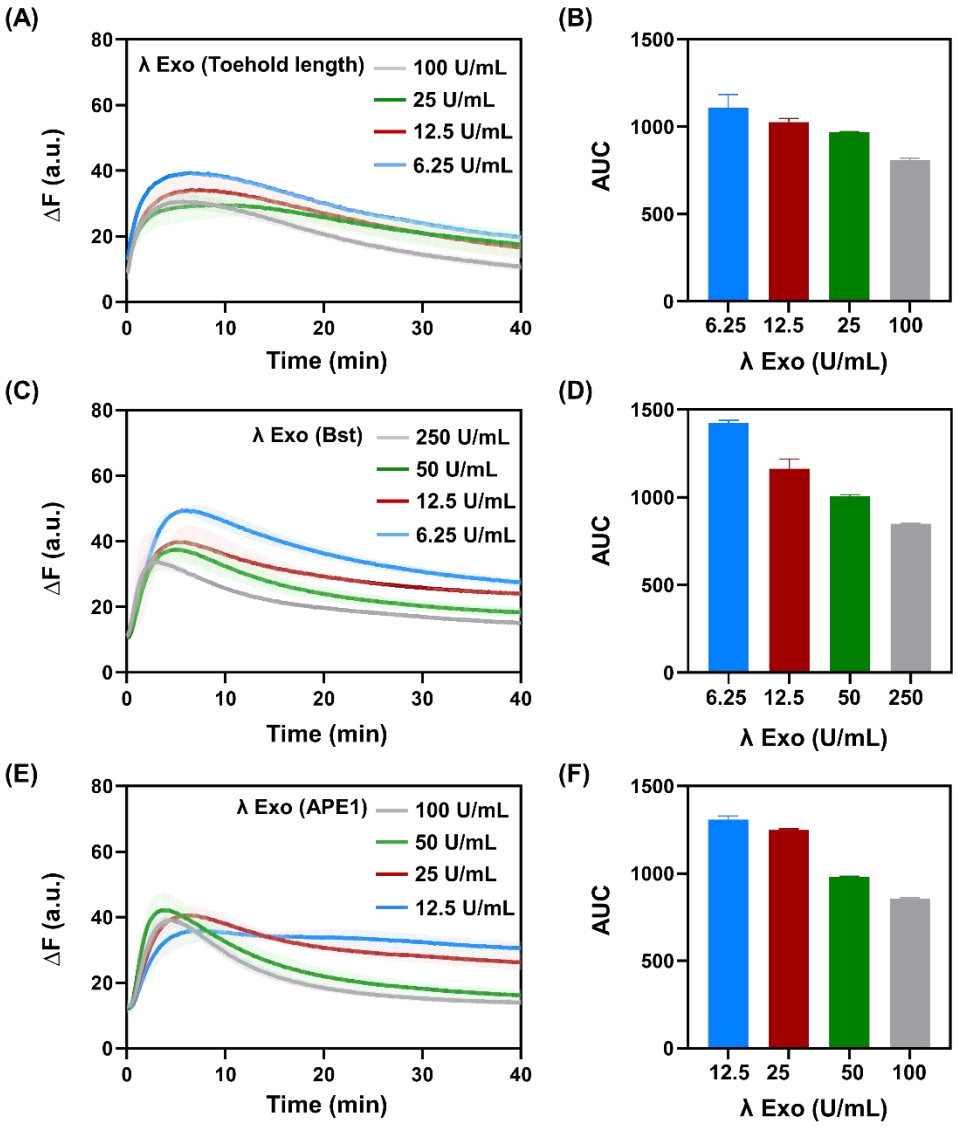

Fig. S6. The strength of the transient state varies with changing concentrations of λ Exo in all fuel flux-controlled dissipative systems. (A) Time-course fluorescence of dissipative system with λ Exo-controlled fuel flux. The toehold length was 10 nt. (B) AUC extracted from panel A. (C) Time-course fluorescence of dissipative system with λ Exo-controlled fuel flux. The concentration of Bst was 160 U/mL. (D) AUC extracted

from panel C. (E) Time-course fluorescence of dissipative system with λ Exo-controlled fuel flux. The concentration of APE1 was 1000 U/mL. (F) AUC extracted from panel E. The concentration of DNA strands in all reaction systems was 50 nM, the temperature was 25 ° C, and the reaction time was 60 min. ΔF is the result by subtracting the initial fluorescence. Error bars in A, B, C, D, E, and F are mean±S.D. from three independent replicates.

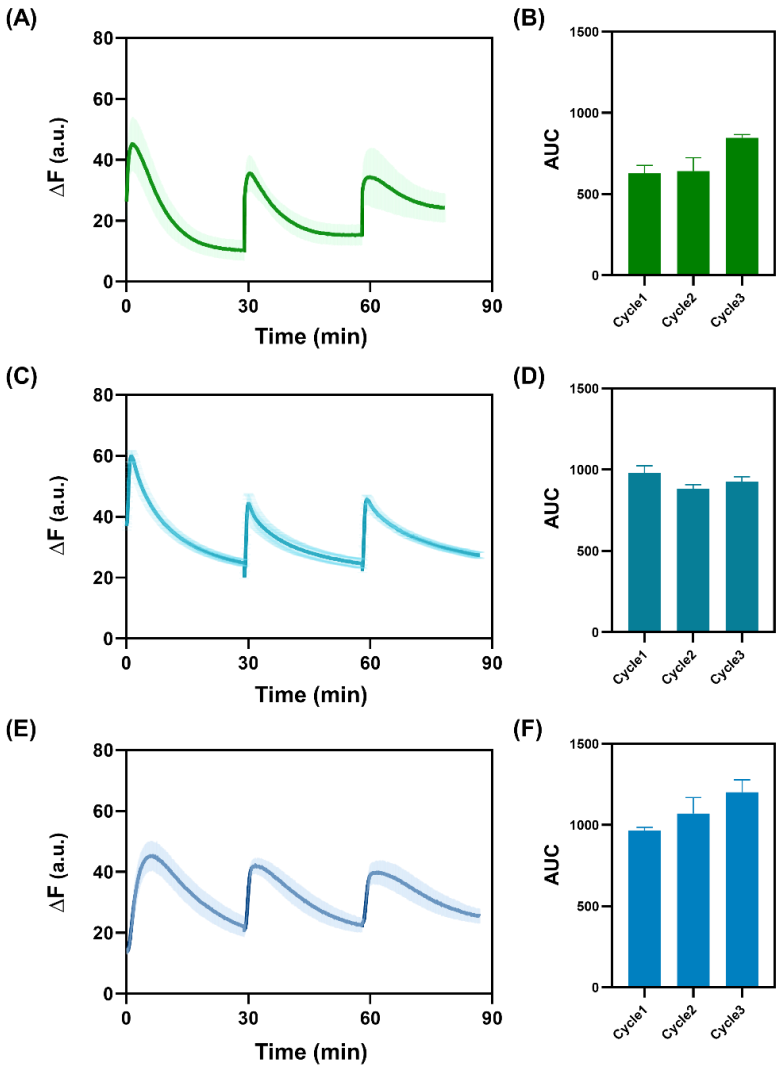

Fig. S7. Multiple-cycle operation of the dissipative system. (A) Time-course fluorescence of a multiple-cycle dissipative system with TMSD-controlled fuel flux. The toehold length was 10 nt. The concentration of λ Exo was 100 U/mL. (B) AUC extracted from panel A. (C) Time-course fluorescence of a multiple-cycle dissipative system with Bst-controlled fuel flux. The concentration of Bst was 160 U/mL. The

concentration of λ Exo was 250 U/mL. (D) AUC extracted from panel C. (E) Time-course fluorescence of a multiple-cycle dissipative system with APE1-controlled fuel flux. The concentration of APE1 was 1000 U/mL. The concentration of λ Exo was 100 U/mL. (F) AUC extracted from panel E. The concentration of DNA strands in all reaction systems was 50 nM, and the reaction temperature was 25 ° C. The trigger strands or structures were added at 0, 30, and 60 min. ΔF is the result by subtracting the initial fluorescence. Error bars in A, B, C, D, E, and F are mean±S.D. from three independent replicates.

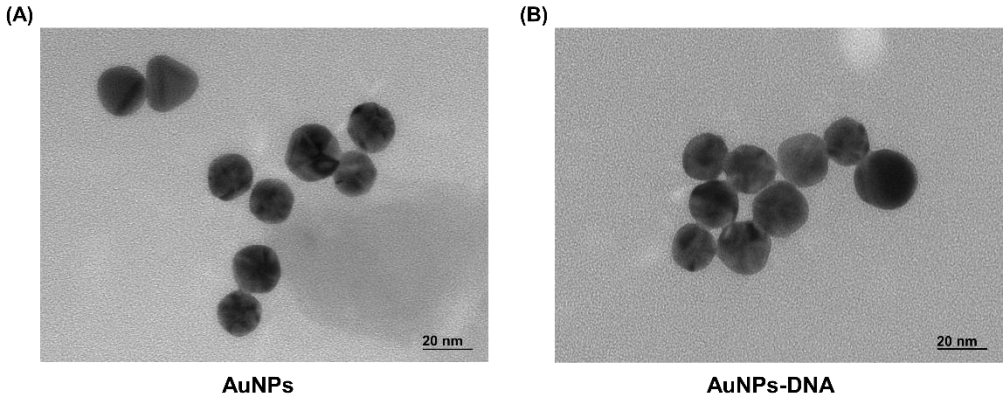

Fig. S8. (A) TEM images of AuNPs. (B) TEM images of ssDNA-modified AuNPs. The scale bar is 20 nm.

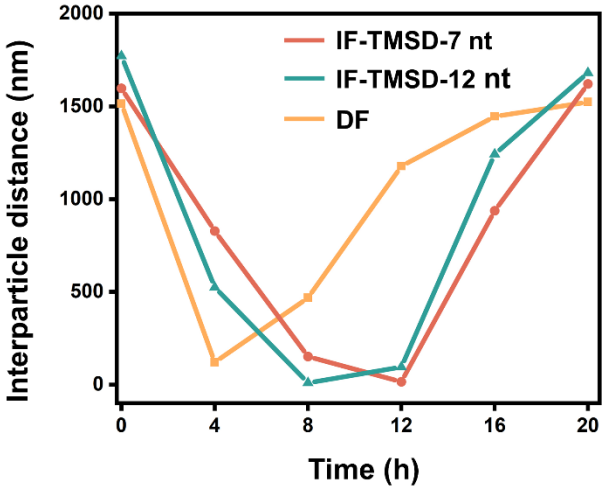

Fig. S9. The interparticle distance of AuNPs in the aggregates in Fig. 5A as a function of time. From the central-most particle in the image, 20 different particles in various directions were to be selected, and the interparticle distance was to be measured.

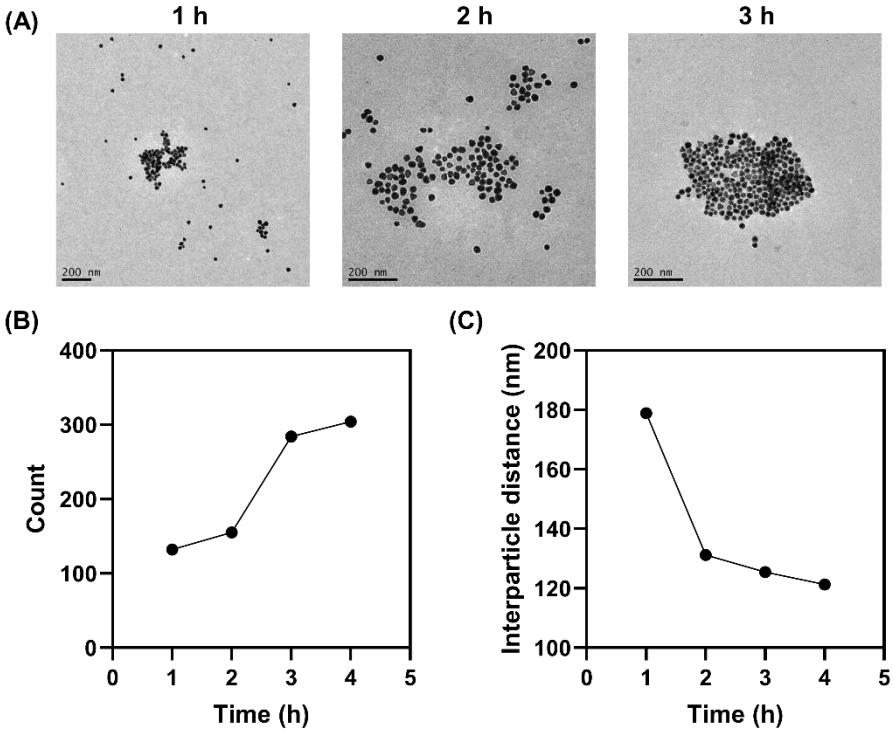

Fig. S10. (A) The TEM images of the assembly state of AuNPs within 0-3 h for the DF group in Fig. 5A. (B) Counts of the number of AuNPs in the aggregates in panel A and Fig. 5A at different times. (C) The interparticle distance of AuNPs in the aggregates in panel A and Fig. 5A at different times.

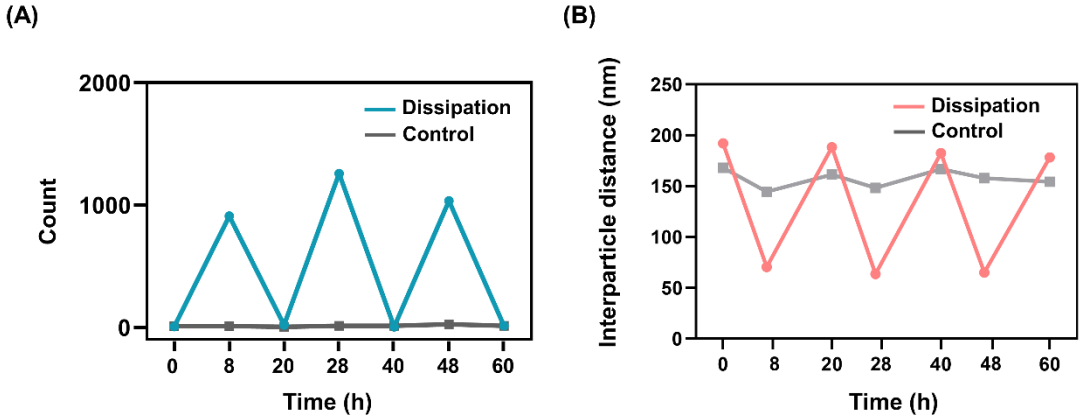

Fig. S11. Particle count and interparticle distance during the dynamic regulation of AuNPs assembly and disassembly for three cycles (Fig. 5E). (A) Counts of the number of AuNP in the aggregates in Fig. 5E as a function of time. (B) The interparticle distance

of AuNPs in the aggregates in Fig. 5E as a function of time. The reaction temperature was 25 °C, the concentration of AuNPs was 5 nM, the concentration of DNA was 5 μM.

References

1 H. P. Erickson and E. T. O'Brien, *Annu. Rev. Biophys. Biomol. Struct.*, 1992, **21**, 145–166.

2 R. H. Wade, *Mol. Biotechnol.*, 2009, **43**, 177–191.

3 T. J. Mitchison, *Science,* **1993**, *261*.

4 G. M. Alushin, G. C. Lander, E. H. Kellogg, R. Zhang, D. Baker and E. Nogales, *Cell*, 2014, **157**, 1117–1129.

5 Y. Liu, S. Fu, J. Liu and X. Su, *Chem. Eur. J.*, 2023, **29**, e202301156.

6 N. Li, Y. Zhao, Y. Liu, Z. Yin, R. Liu, L. Zhang, L. Ma, X. Dai, D. Zhou and X. Su, *Nano Today*, 2021, **41**, 101308.

7 J. Liu, Y. Liu, L. Zhang, S. Fu and X. Su, *Biosens. Bioelectron.*, 2022, **215**, 114561.